General Mechanism for Sulfate Radical Addition to Olefinic Volatile Organic Compounds in Secondary Organic Aerosol

He Ren, Jane A. Sedlak, and Matthew J. Elrod*

Read Online

ACCESS | 📊 Metrics & More | 📰 Article Recommendations | 🆂🆘 Supporting Information

ABSTRACT: Previous laboratory studies have suggested that sulfate radical addition to olefinic biogenic volatile organic compounds (BVOCs) is a potential formation mechanism for some organosulfates detected in ambient secondary organic aerosol (SOA). However, these studies propose conflicting reaction products, possibly because laboratory dissolved oxygen levels did not accurately reflect atmospheric conditions. Additionally, these studies used analytical methods that could not definitively identify and quantify the structurally specific products. Here, we describe a method that allows for the study of the reaction of sulfate radicals and several olefinic precursors, including allyl alcohol (AA), methyl vinyl ketone (MVK), 2-methyl-3-buten-2-ol (MBO), and methacrolein (MA), with careful control of dissolved oxygen levels and using the isomer-specific nuclear magnetic resonance (NMR) method to definitively identify and quantify the reaction products. Specific mechanisms for each olefinic precursor were developed, as well as a generalized mechanism that can be used to predict the sulfate radical reaction pathways for any olefin. The product yield results indicate that this mechanism is dominated by carbon backbone fragmentation pathways: 61, 83, 79, and 100% for AA, MVK, MBO, and MA, respectively. Several of the observed organosulfate products have also been detected in field observations of SOA, which indicates the potential relevance of this mechanism in the atmosphere.

KEYWORDS: sulfate radicals, alkenes, secondary organic aerosol, nuclear magnetic resonance
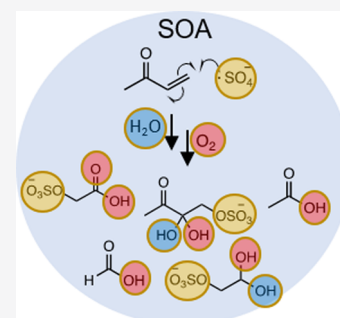
INTRODUCTION

Secondary organic aerosol (SOA) is a major type of atmospheric aerosol, which is mostly formed from the oxidation of biogenic volatile organic compounds (BVOCs) in the atmosphere followed by partitioning into the condensed phase.[1] These oxidized chemical compounds can undergo further reactions in the particle phase, thus changing the composition and optical properties of SOA, which has important ramifications for Earth's climate[2] and human health.[3−5] Organosulfates are estimated to contribute up to 15% of the total SOA mass in several sites across the United States.[6−8] From the high-resolution mass spectrometry-derived molecular formulas identified in field studies, it is apparent that many BVOCs are potential precursors for the formation of organosulfates, including isoprene, monoterpenes, sesquiterpenes, and 2-methyl-3-butene-2-ol.[8−13]

While the formation of some major isoprene-derived organosulfates has been associated with the acid-catalyzed ring-opening reactions of isoprene-derived epoxides with the sulfate anion (SO_4^{2-}),[14−16] the atmospheric detection of small and/or highly oxidized organosulfates suggests the existence of free radical-initiated oxidative organosulfate-forming processes. It has been shown that the OH radical can both form highly oxidized and/or fragmented organosulfates from existing organosulfates[17,18] and that these processes can potentially liberate the similarly strong oxidant, sulfate radical anion $(\cdot SO_4^-)$.[17] There have also been several mass spectrometry-

based laboratory studies aimed at investigating how sulfate radical addition to olefinic BVOCs might be able to explain some of the organosulfates detected in the atmosphere.[19−22] Previous laboratory investigations have detected organosulfate products, identified by their mass-to-charge (m/z) ratios, that have also been detected during field studies.[8−10] However, these laboratory studies have also detected oligomers that were only observed in bulk phase solution, not in ambient aerosol or chamber experiments.[20,22] The oligomers may have been formed through alkyl radical-initiated chain oligomerization reactions that would not be feasible in oxygen-equilibrated ambient SOA, where the alkyl radical would be expected to rapidly associate with oxygen to form a peroxy radical.[23]

All of the previous laboratory studies of the sulfate radical addition reaction used the method of liquid chromatography high-resolution mass spectrometry (LC−MS), wherein the LC separation component serves to simplify the analysis of complex mixtures and the MS component is a high-sensitivity detection method that can provide an exact molecular formula for the measured products. If standards are available, the LC

retention times and molecular formulas can be used to distinguish among possible isomeric species.[24,25] However, most of the previous work did not have access to standards, which is the likely reason why these studies propose different products and, in some cases, different formation mechanisms for the same reaction systems. While the NMR technique suffers from low sensitivity and is not easily coupled to chromatographic separation techniques, it has the ability to definitively determine molecular structures without the need for standards. The complementary strengths of the LC−MS and NMR techniques have recently been demonstrated by a study of sulfate radical reactions with aromatic compounds in the context of water treatment chemistry, which found that both LC−MS- and NMR-based methods were necessary to elucidate the mechanisms.[26]

Because of the discrepancies between previous studies, a general mechanism for sulfate radical addition to olefinic compounds has yet to be developed. Using the NMR technique to more definitively identify reaction products, we have developed a generalized mechanism by examining several olefinic systems that can explain the formation of a class of highly oxidized and fragmented organosulfates detected by field studies.[8] Based on the specific mechanisms developed for each VOC studied, allyl alcohol (AA), methyl vinyl ketone (MVK), methacrolein (MA), and 2-methyl-3-buten-2-ol (MBO), a general sulfate radical addition mechanism with four possible reaction pathways was developed. Finally, this mechanism was used to try to reconcile the results from the various laboratory studies and to help rationalize the observation of BVOC-derived organosulfates in ambient SOA.

■ MATERIALS AND METHODS

Complementary photochemical and thermal sulfate radical generation methods were both used to study the sulfate radical addition reaction. Photochemical-initiated homolytic cleavage of persulfate ions efficiently generates sulfate radicals; however, the energetic 254 nm irradiation could lead to photolysis of some precursors as indicated by their high molar absorptivity at 254 nm (Figure S1) and possibly photolysis of some products. Thus, a thermal technique was used to identify potential artifacts in the photochemical system arising from non-actinic 254 nm photolysis.

The continuous oxygen flow throughout the photochemical experiment and the pure oxygen headspace of the sealed vial in the thermal experiment were designed to ensure atmospherically relevant dissolved oxygen levels. The sealed thermal experiment also allows for the potential identification of volatile potential products lost from evaporation in the photochemical experiment. To obtain unambiguous structural information, ^1H, ^{13}C, and correlation NMR spectroscopies were used to characterize the products. Products were also quantified to obtain the branching ratios for the proposed mechanism of each system.

Photochemical Experiments. Photochemical reactions were carried out in a Sigma-Aldrich micro-photoreactor[27] with a water-cooled mercury pen lamp (λ_{max} = 254 nm) to initiate the homolytic cleavage of the peroxide O−O bond. All reactions were run at room temperature. In the sulfate radical experiments, sodium 2,2-dimethyl-2-sila-pentane-5-sulfonate (DSS, 6.9 mM) and potassium persulfate ($K_2S_2O_8$, 50 mM) were added to 5 mL of D_2O. The solution was mixed until both solids were dissolved before being transferred into the photochemical reactor and oxygenated for 15 min at a flow

rate of 0.10 SLPM without irradiation. The oxygen-saturated state of the solutions was confirmed by measurement of the dissolved oxygen levels. The oxygenated solution was then removed from the reactor, and the olefin, methyl vinyl ketone (MVK, 0.20 M), 2-methyl-3-buten-2-ol (MBO, 0.10 M), or allyl alcohol (AA, 0.10 M), was added to the solution and stirred for 5 min before the sample was returned to the reactor and irradiated for 50−60 min with a continuous oxygen flow through the photoreactor. These concentrations were chosen because they are the minimum values that allowed for sensitive NMR analysis. The reaction time was chosen so that 25% of reactant remained in order to avoid secondary sulfate radical reactions with product species while maximizing product yields. For each olefin photochemical experiment, the sample preparation and experimental apparatus were the same, but the reactant, irradiation time, and oxygen gas flow rate were modified.

In the low-oxygen AA control photochemical experiments, nitrogen was bubbled through the photoreactor instead of oxygen. Dissolved oxygen measurements indicated levels of ≤ 2 mg/L (compared to 8 mg/L for air equilibrated solutions). In the OH radical reaction with MVK control experiment, 50 mM H_2O_2 solution was made instead of $K_2S_2O_8$ solution. In the persulfate-free MA control experiment, $K_2S_2O_8$ was not added.

Long-Term Thermal (LTT) Experiments. For each olefinic compound, "O_2 regular" and "O_2 control" reaction conditions were examined. In the "O_2 regular" experiments (the standard photochemical experiment conditions), $K_2S_2O_8$ was used to generate sulfate radical thermally. The "O_2 control" experiment served as a $K_2S_2O_8$ control (no $K_2S_2O_8$ added) for the standard "O_2 regular" experiment to determine if the olefinic precursor had other potential non-sulfate radical reaction pathways. For each reaction condition, four to six sealable 20 mL sample vials were prepared and sealed at the same time. At various time points after sealing, a vial was selected and analyzed via NMR to provide kinetics data and determine the optimal reaction time for the next vial to be analyzed. Each vial contained 1 mL of an oxygenated solution of D_2O with DSS (6.9 mM), or $K_2S_2O_8$ (50 mM, omitted in the "O_2 control" experiments). The olefinic precursors, MVK (0.10 M), MBO (0.10 M), or MA (0.20 M), were added to the vial and mixed via a shaker plate for 5 min. Then, the solution was oxygenated for 1 min at 0.20 SLPM with a custom-built flow-through cap assembly. The vial was then sealed and later reopened for the measurement of the dissolved oxygen level by a Vernier Go Direct optical dissolved oxygen probe and for NMR analysis.

Reagents used in the experiments were obtained from Millipore-Sigma: MVK (99%, purified by vacuum distillation), MBO (98%), AA (99%), MA (95%), $K_2S_2O_8$ (99%), and H_2O_2 (30 wt % in H_2O); and from Cambridge Isotope Laboratories, Inc.: DSS (97%) and D_2O (99.5%, 99.9% D).

NMR Methods. All the samples were analyzed using a Bruker 400 MHz NMR. Both proton and carbon chemical shifts were calibrated using the terminal methyl protons or methyl carbons of DSS. The concentration of each product was determined using the proton-weighted ratio of the product integration to the DSS standard. Distortionless enhancement by polarization transfer (DEPT) experiments were used to help establish the number of protons bonded to each carbon atom. Due to the low concentration of products, ^{13}C NMR, DEPT 135, and DEPT 90 spectra were taken with 23,000 scans. ^1H-^{13}C single- (HSQC) and multi- (HMBC) bond
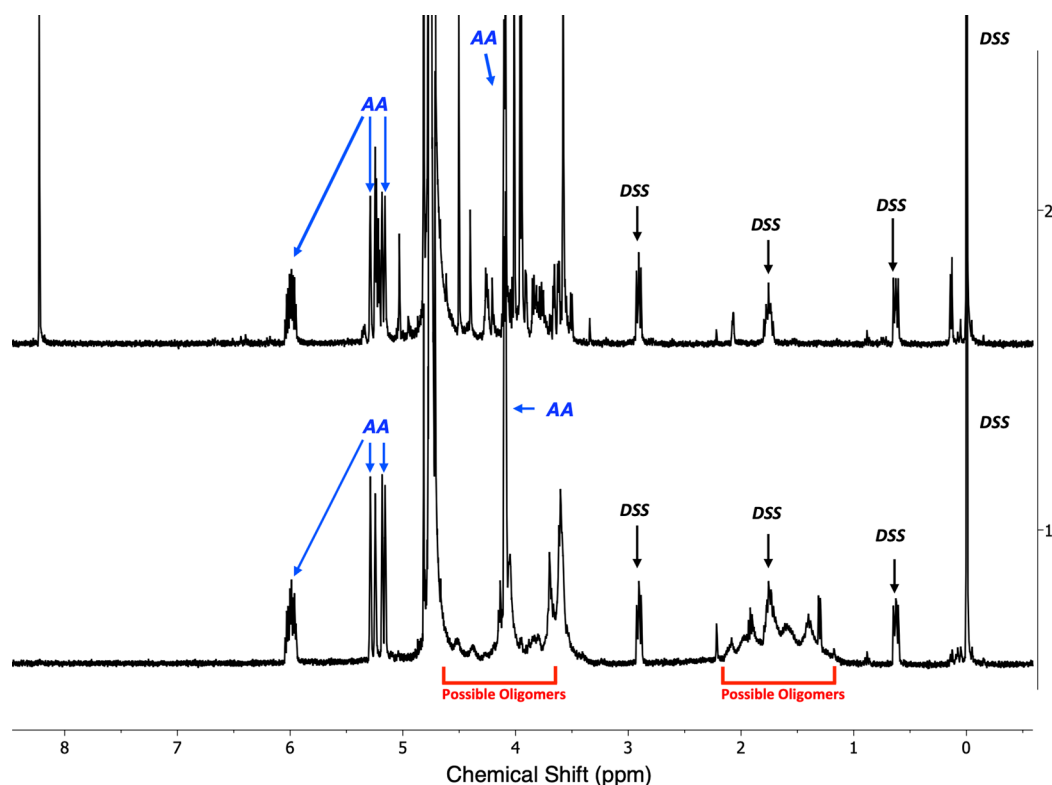
Figure 1. ^{1}H-NMR spectrum of the oxygen-saturated AA experiment (after 60 min of irradiation) (top) compared to a ^{1}H-NMR spectrum of the low-oxygen AA experiment (after 45 min of irradiation) (bottom). The broad peaks (due to the presence of a large number of chemically similar but structurally unique protons) in the low-oxygen experiment indicate the presence of oligomers.

correlation spectra were collected to not only help to provide longer-range bond connectivity information but also to uncover overlapping signals in the single-dimensional ^{1}H or ^{13}C spectra, thus significantly enhancing the power of the NMR technique for the analysis of complex mixtures. The HSQC or HMBC spectra were collected with 90 and 170 scans and pulse sequences of hsqcetgpsi2 and hmbcgplpndqf, respectively. Products were identified by comparing the detected chemical shifts with standards in the lab's NMR D$_2$O database and an online NMR CDCl$_3$ database.[28] For products for which proton and carbon chemical shift data were not available, shifts were predicted based on the general chemical shift trends for similar species.[29]

■ RESULTS AND DISCUSSION

AA + SO$_4^-$ Photochemical System. Allyl alcohol was used to determine the optimal photochemical reaction conditions given its simple structure, low molar absorptivity at 254 nm, and low volatility. The role of oxygen levels in the formation of oligomers was investigated by conducting one experiment flowing pure O$_2$ through the reactor, the oxygen-saturated trial, and another experiment with pure N$_2$, the low-oxygen trial. A comparison of the resulting ^{1}H-NMR clearly illustrates that oligomerization does not occur under oxygen-saturated conditions but does occur under low-oxygen conditions (Figure 1). This shows that dissolved oxygen levels must be carefully controlled in order to produce atmospherically relevant products, given that ambient aerosols are likely to be oxygen-saturated systems due to their high surface area to volume ratios.

Several highly oxidized and/or fragmented organosulfates produced in the oxygen-saturated experiment were identified,

including glycerol-1-sulfate, DHA-S/DHA-S-H (dihydroxyacetone-1-sulfate/dihydroxyacetone-1-sulfate hydrated), and GL-S-H (glycoaldehyde-2-sulfate hydrated). The annotated ^{13}C NMR spectra are shown in Figures S1 and S2, a summary of product yields is shown in Table S2, and the proposed mechanism is shown in Figure S3.

MVK + SO$_4^-$ Photochemical System. The proposed mechanism for sulfate radical addition to MVK, given in Figure 2, was developed based on products identified by NMR (Figures S4−S5) and rationalized using oxidative gas-phase radical mechanisms as a guide.[30] The reaction between the sulfate radical and an olefin begins with radical addition to the double bond to form an alkyl radical. If the double bond is not symmetrically substituted, the sulfate radical will preferentially add to the less substituted side due to lower steric hindrance and the higher stability of the resulting substituted alkyl radical. In gas-phase atmospheric radical reactions, the oxygen molecule rapidly adds to the alkyl radical to form a peroxy radical.[30] In the absence of NO$_x$, the alkyl peroxy radical is then expected to undergo a series of self-reactions − this series of self-reactions was observed for the sulfate radical reactions.[23]

Several other reaction pathways such as the hydration of carbonyl compounds and the sulfate radical addition to the nonterminal position of the double bond were also considered as a possibility for all BVOC systems, but no unique products that could provide evidence for a pathway with sulfate radical addition to the more substituted position were observed in any of the experiments.

The annotated HSQC and HMBC spectra of the MVK + SO$_4^-$ photochemical reaction are given in Figures S4 and S5, which were used to confirm the structural assignments given in Figure 2. Several products from Paths 1 and 2 were observed,
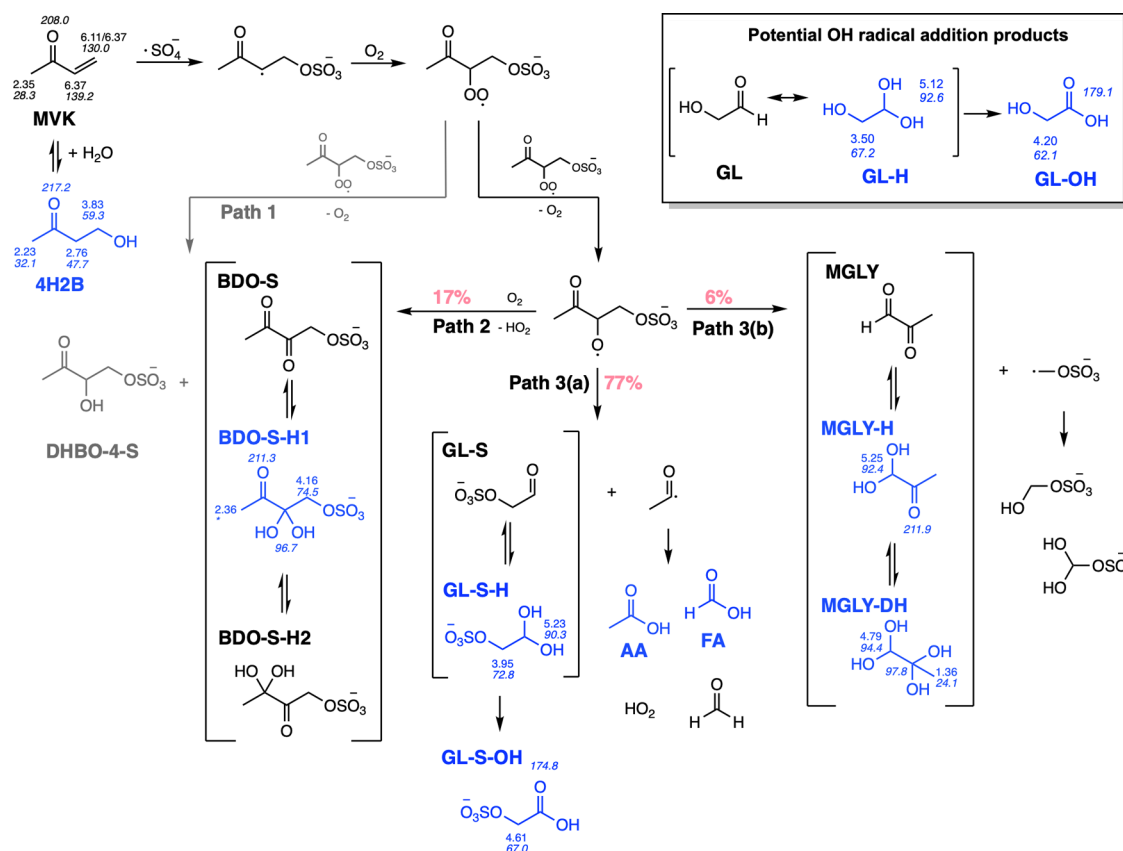
Figure 2. Proposed mechanism for sulfate radical addition to MVK. Observed products (with their ^{1}H and/or ^{13}C NMR chemical shifts indicated) are labeled in blue, while unobserved pathways are labeled in gray. The branching ratios of the photochemical experiment are listed for each leg of reaction in pink.

including 4-sulfate-2,3-butanedione 3-hydrated (BDO-S-H1), methylglyoxal monohydrated (MGLY-H), methylglyoxal dihydrated (MGLY-DH), GL-S-H, acetic acid (AA), and formic acid (FA). A summary of the product concentrations is listed in Table S3. The chemical shifts were not available for DHBO-4-S and were instead predicted using the methods described above, but the predicted peaks were not observed. This result does not indicate that DHBO-4-S was not formed, but rather we were unable to identify it due to either an inaccurate prediction algorithm or a concentration just below our detection limit. In the absence of DHBO-4-S, the only unique product of Path 1, Path 1 was presumed to be inactive and BDO-S-H1 was assumed to form via Path 2 exclusively. The observation of the fragmented species GL-S-H, MGLY-H, and MGLY-DH indicated that both Path 3(a) and Path 3(b) were active.

Several products from pathways other than sulfate radical addition pathway initiated by RO$_2$ self-reaction were also observed, such as 4-hydroxy-2-butanone (4H2B), glycolaldehyde hydrated (GL-H), glycolic acid-2-sulfate (GL-S-OH), and glycolic acid (GL-OH). 4H2B is a possible MVK hydration product formed via the enol tautomer (Figure S6). Glycolaldehyde (the unhydrated form of GL-H) is a product of the OH-oxidation of MVK in the gas phase[31] and aqueous[21] phase. It is possible that the GL-H observed in this experiment could come from a OH radical addition equivalent of Path 3(a) (Figure 2). A potential source of OH radicals is the reaction between acyl peroxy radicals and HO$_2$.[23] To test the hypothesis that GL-H was a product of OH radical addition to MVK, an experiment was carried out in which the photo-

chemically initiated homolytic cleavage of H$_2$O$_2$ served as a source of OH radicals. GL-H and GL-OH were observed as products of this reaction, which indicates that OH radical addition to MVK can be used to rationalize the formation of these compounds.

The formation of GL-S-OH and GL-OH suggests that GL-S/GL-S-H and GL/GL-H underwent secondary oxidation in the solution, likely via a R(O)O$_2$ + HO$_2$ pathway. Some secondary reactions could be photochemical reactions, such as the photolysis of the unhydrated aldehyde, or could be initiated by the aldehydic hydrogen abstraction reactions with sulfate or OH radicals in the solution. In these cases, the results from long-term thermal reactions (described in the next section) provide a way to help distinguish potential photochemical artifacts from non-photochemical processes that are potentially atmospherically relevant.

AA, FA, and formaldehyde are hypothesized to come from the acetyl radical in Path 3(a), which is the complementary fragment of GL-S in the sulfate radical addition pathway and GL in the OH radical addition pathway. Thus, the sum of the concentrations for these three compounds was expected to be equivalent to the sum of their complementary products. However, the concentration of the small organic compounds was much higher than their complementary products, which might be caused by unaccounted for secondary reactions of GL-S/GL. It is also possible that other formation pathways for these small organics exist.

The presence of OH radical reactions led to a complication in calculating branching ratios because MGLY can be formed by both sulfate radicals, Path 3(b) and OH radicals, a Path
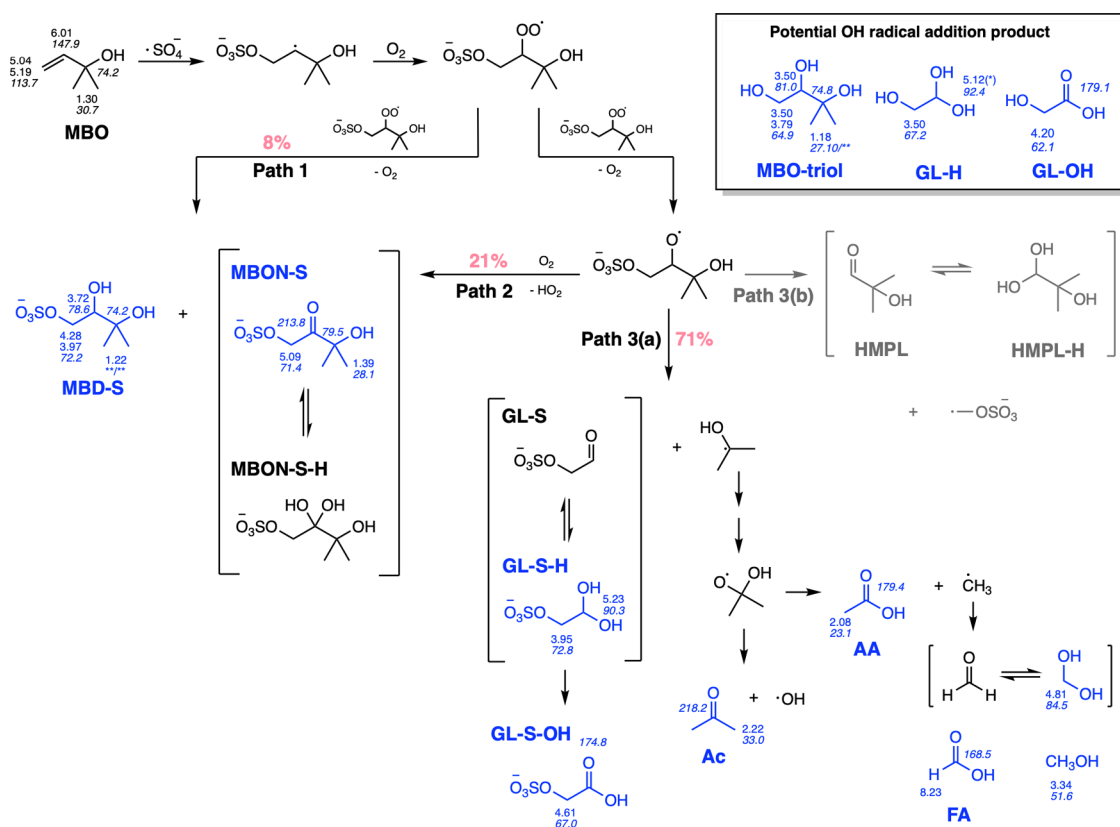
Figure 3. Proposed mechanism for the sulfate radical addition to MBO. Observed products (with their ^{1}H and/or ^{13}C NMR chemical shifts indicated) are labeled in blue, while unobserved pathways are labeled in gray. The branching ratios of the photochemical experiment are listed for each leg of reaction in pink.

3(b)-like series of reactions initiated by the OH radical as opposed to the sulfate radical. Therefore, to calculate the branching ratio of the sulfate radical addition to MVK, the potential sources of MGLY were considered according to three assumptions. In case 1, MGLY-H and MGLY-DH were assumed to come from the sulfate radical addition pathway only. In case 2, they were assumed to come from the OH radical addition pathway only. In case 3, the contribution of the sulfate radical addition reactions to the formation of MGLY-H and MGLY-DH was assumed to be the same as the ratio of the corresponding sulfate/OH radical addition reaction products from Path 3(a) (in other words, the branching ratio between Paths 3(a) and 3(b) was assumed to be the same for both OH- and sulfate-radical-initiated pathways). A comparison of the results of these three cases (Table S4) indicates that this uncertainty about the formation routes for MGLY-H and MGLY-DH has a minor effect on the calculated branching ratios for the overall mechanism, but case 3 was selected as the most likely scenario. Using this scenario, the branching ratio between Path 2, Path 3(a), and Path 3(b) in the photochemical reaction is 17%:77%:6%.

MVK + SO$_4^-$ LTT Reaction. All of the products identified in the photochemical experiments were also observed in the LTT O$_2$ regular experiment (Table S5). As discussed earlier, the major advantage of the slow thermal generation of sulfate radicals is to avoid the potential photochemical artifacts brought about by the energetic 254 nm light. Although this does not rule out all photochemical artifacts, the identification of GL-S-OH and GL-OH in both the photochemical and LTT experiments suggests that the H-abstraction reactions of the

GL-S and GL were due to radical reactions. The abstraction reaction does not lead to the incorporation of unique functional groups because both sulfate- and OH-radical-initiated abstraction of the aldehydic hydrogen atom will lead to the same product, so the identity of the oxidizing radical could not be determined.

However, the long reaction time clearly led to complications like the extensive hydration of MVK to 4H2B. Under the weakly acidic conditions of the sulfate-radical generating experiments (see Table S6), approximately half of the reactants were hydrated after 74 days (Figure S7). Over the same time period, approximately 35% of the MVK was converted to 4H2B even in the relatively pH neutral environment of the radical-free control experiment. This hydration reaction leads to lower amounts of MVK available for the sulfate radical addition reaction and produces OH radicals, which lead to secondary reactions. However, the measurement of dissolved oxygen levels indicated that vials were sufficiently sealed such that oxygen was not able to move in or out of the vials over the several-month time frame, and therefore, we conclude that the LTT results were not compromised by the loss of volatile components.

Another complication in the thermal generation of sulfate radicals shared by all olefinic systems was the increase in the importance of OH-radical-initiated reactions as compared to the photochemical experiments (Table S6). The persulfate undergoes hydrolysis in dilute acidic solutions through the following reaction[32]
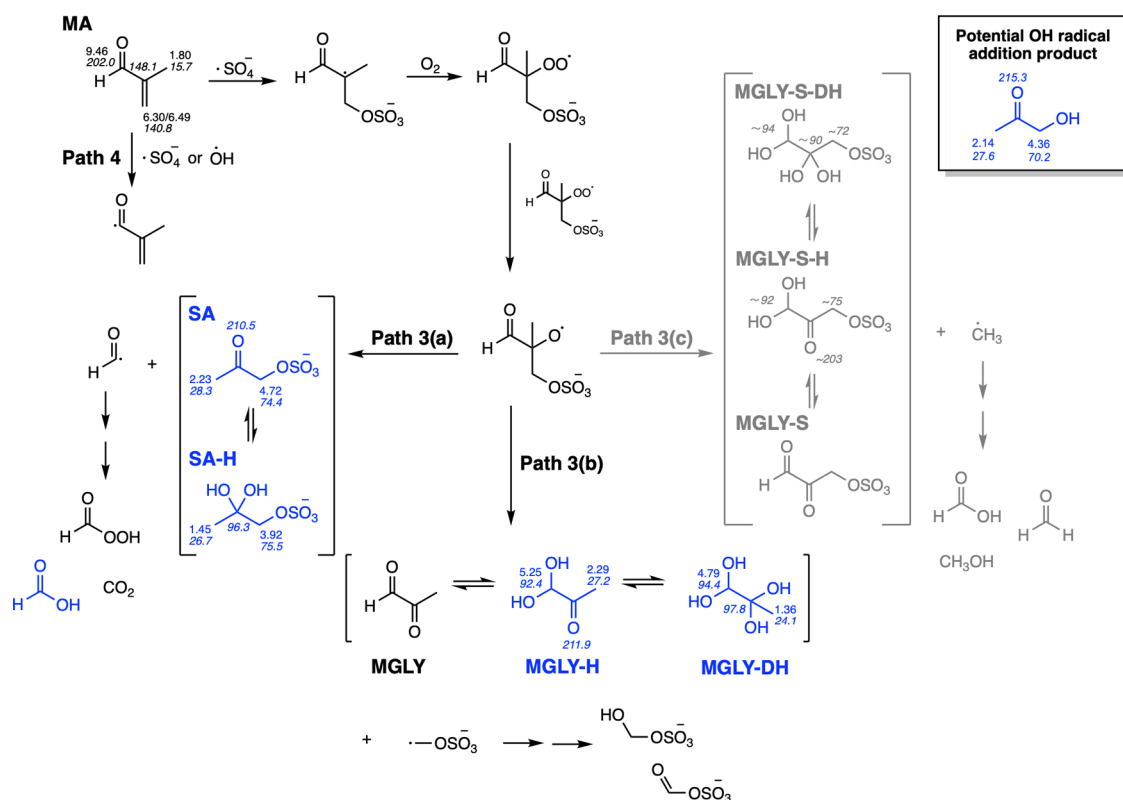
$$S_2O_8^{2-} + 2H_2O \rightarrow 2HSO_4^- + H_2O_2 \tag{1}$$
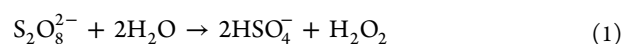
Figure 4. Sulfate radical addition to MA mechanism. Path 4 is elaborated in Figure S18. Observed products (with their ^{1}H and/or ^{13}C NMR chemical shifts indicated) are labeled in blue, while unobserved pathways are labeled in gray.

The rate constant at pH = 1.3 was previously determined to be 6.12×10^{-6} min^{-1}. Therefore, the formation of hydrogen peroxide and its thermal homolytic cleavage could have provided a source of OH radicals in the LTT experiments.

The branching ratios for the LLT experiments were calculated using the same method used to analyze the product distribution of the photochemical experiments (Tables S7–S9). The LTT generation of sulfate radicals resulted in a different product distribution from the photochemical experiments. This is likely due to the more extensive secondary reactions and OH radical complications under the LTT conditions that were favorable on the several-month time scale of the LLT experiments compared to the 1 h time scale of the photochemical experiments. However, the LTT experiments allowed for the definitive identification of the primary sulfate-radical-initiated processes in the photochemical experiments.

MBO + SO$_4^-$ Photochemical Reaction. The sulfate radical reaction with MBO was found to proceed following a similar mechanism to the one developed for MVK (Figure 3). The addition of the sulfate radical to the unsubstituted carbon in the double bond of MBO followed by the RO$_2$ self-reaction was found to be the dominant reaction pathway based on the HSQC and HMBC spectra (Figures S8–S10). A complete product summary and quantification are given in Table S10. The observation of 2-methyl-4-sulfate-butan-2,3-diol (MBD-S), 2-hydroxy-2-methyl-4-sulfate-3-butanone (MBON-S), GL-S-H, acetone (Ac), AA, and FA indicates that Path 1, Path 2, and Path 3(a) are active. The product from Path 3(b), 2-hydroxy-2-methylpropanal (HMPL), has been detected in the gas-phase OH oxidation of MBO,[33] but the predicted chemical shifts for both hydrated and unhydrated HMPL were not detected in this experiment.

Like the MVK system, possible OH radical addition products, 2-methyl-butan-2,3,4-triol (MBO-triol) and GL-H, were also detected. However, 2,4-dihydroxy-2-methyl-3-butanone, the complementary product of MBO-triol in Path 1 and the OH-addition equivalent product from Path 2, was not observed either due to its low concentration (more likely) or to the inaccuracy of the chemical shift prediction method because reference standards were not available (less likely). In addition, the secondary products GL-S (GL-S-OH) and GL (GL-OH) were also observed.

From the product concentrations, the branching ratio between Path 1, Path 2, and Path 3(a) in the photochemical reaction is determined to be 8%:21%:71%.

MBO + SO$_4^-$ LTT Reaction. The sulfate radical addition mechanism for MBO in the LTT oxygen-rich experiments was expected to be similar to the proposed mechanism in Figure 3. Although most of the products produced in the photochemical experiment were also observed in these LTT experiments (a complete summary is given in Table S11), there were some differences in the product distribution. GL-S-OH, the product from the secondary reaction of GL-S-H, was observed in the photochemical reaction but not in LTT reactions. This is most likely due to a low concentration of GL-S-OH and/or overlapping NMR signals. Unlike MVK hydration, 3-methyl-2-butene-1-ol (MB-1-O), a hydration product of MBO, was identified in the weakly acidic reactive system experiments but not in the neutral nonreactive control experiments, which suggests that the formation of MB-1-O is acid-catalyzed (Figure S12, Table S12 provides experiment parameters including pH estimates).

The only OH radical addition product identified in LTT reactions was MBO-triol. At 94 days and 144 days of the
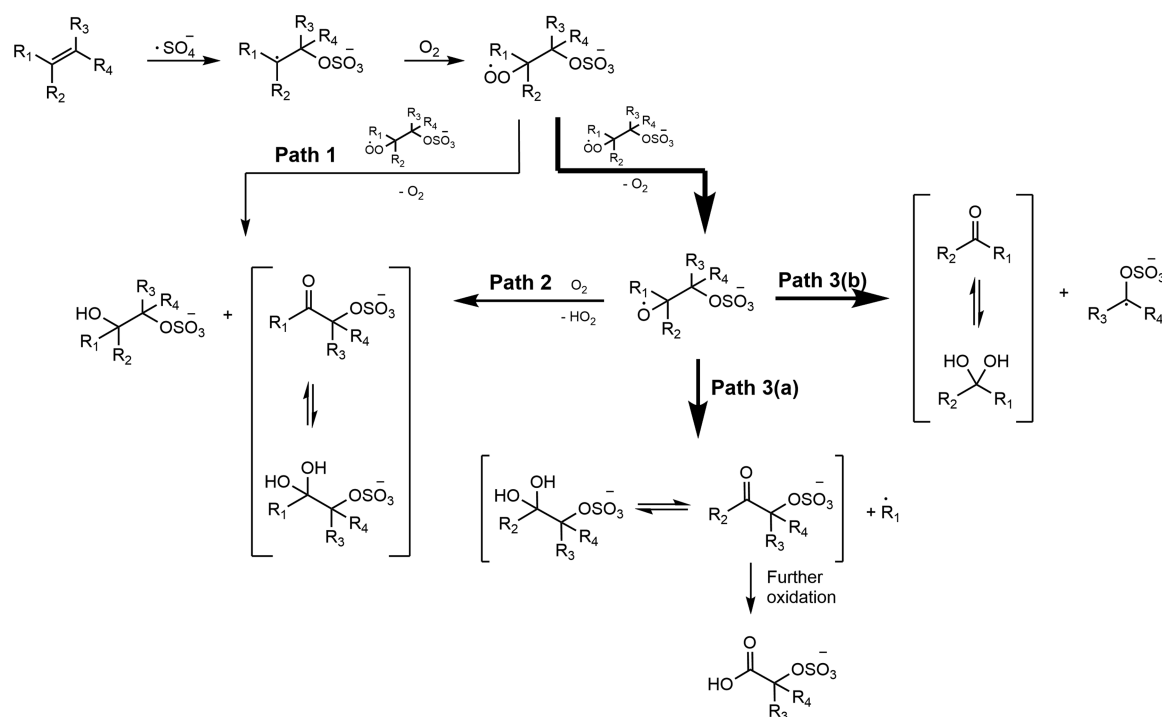
Figure 5. General sulfate radical addition mechanism. The relative importance of the pathways is indicated by the relative sizes of the reaction arrows.

reactive system experiments, the formation of MBO-triol was the dominant reaction pathway (Figure S11). The complementary product 2,4-dihydroxy-2-methyl-3-butanone of MBO-triol in Path 1 was still not observed. Its absence raises some concerns about attributing the formation of MBO-triol solely to the OH-radical-initiated RO_2 self-reaction pathway. One alternative hypothesis is that dihydroxylation at the MBO double bond could occur through the hydrolysis of an epoxide intermediate, presumably formed via a peroxide oxidant.[13,34]

Due to the higher concentration of MBD-S than MBON-S after 54 days for the reactive system experiments, the branching ratio for Path 2 became negative (Table S13). One possible explanation is that there might be another formation pathway for MBD-S, which could be similar to the non-peroxy radical self-reaction formation of MBO-triol. Thus, the LTT results for the MBO system were mainly used to gain insight into potential complications in the photochemical experiments, much the same way that the LLT experiments were used for MVK.

MA + SO_4^- LTT Reaction. MA was observed to undergo significant photolysis under the photochemical reaction conditions, which is consistent with its high molar absorptivity at that wavelength (Figure S13).[35] Thus, the photochemical reaction method could not be used, and LTT experiments were instead used to study the reactions between sulfate radicals and MA despite the aforementioned complications of the thermal method.

The addition of the sulfate radical to the terminal carbon atom in the double bond of MA under oxygen-rich conditions is expected to be similar to the other olefinic precursors, but the tertiary peroxy radical is unable to proceed through peroxy radical self-reaction (Path 1) or the H-abstraction reaction of the alkoxy radical (Path 2). The proposed sulfate radical addition mechanism for MA followed by the RO_2 self-reaction is shown in Figure 4 based on the HSQC and HMBC spectra

of experiments collected after 60 days (Figures S14−S15). Product summaries (Tables S14−S15) and ratios (in Table S16) are plotted as a function of time (Figures S16−S17). The radical addition to MA could lead to autooxidation of the peroxy radical[36] and the formation of SA, a shared product with Path 3(a).

Another potential reaction pathway of MA involves the abstraction of the aldehydic hydrogen by the oxidizing radical (Path 4). Based on the gas-phase OH-radical H-abstraction schemes[37] and general peroxy radical reactions,[23] the H-abstraction by sulfate or OH radical mechanism in the aqueous phase is proposed (Figure S18). While this pathway could be important in understanding the atmospheric chemistry of MA, the abstraction pathway will not lead to the direct formation of organosulfates.

The observation of sulfatoacetone (SA) and MGLY-H/MGLY-DH indicates that Path 3(a) and Path 3(b) are active. This result is consistent with the recent identification of a TiO_2-mediated photochemical pathway for the formation of sulfatoacetone from methacrolein.[38] For Path 3(c), the chemical shifts of methylglyoxal-3-sulfate hydrated (MGLY-S-H) and methylglyoxal-3-sulfate dihydrated (MGLY-S-DH) were predicted but not identified. The observation of methacrylic acid (MA-OH) and AA suggests that the aldehydic abstraction pathway is active. The presence of hydroxyacetone (HA) indicates that the OH radical likely adds to the terminal carbon atom in the double bond of methacrolein, following a path similar to Path 3(a) or undergoing the autooxidation reaction that led to the formation of SA.

Like the MVK system, in the MA system, MGLY and its hydrated forms are shared products between the sulfate and the OH radical addition pathways. To determine branching ratios, the contributions of the sulfate radical and OH radical to the formation of MGLY were approximated with two cases: (1) all of the detected MGLY-H and MGLY-DH were

assumed to come from the sulfate radical addition pathway only, and (2) the contribution of the sulfate radical addition reactions to the formation of MGLY-H and MGLY-DH was assumed to be the same as the ratio of the corresponding sulfate/OH radical addition products from Path 3(a) (i.e., the ratio of ([SA] + [SA-H]) to [HA]), which is known. The branching ratios between Path 3(a) and Path 3(b) of O_2 regular experiment for both trial 1 and trial 2 are listed in Table S17. One reason attributed to differing results between trial 1 and trial 2 is the difference in average initial MA concentration (58 vs 150 mM). This was due to the difficulty in delivering reproducible amounts of volatile MA to the reaction vials. The contribution of unimolecular autooxidation is potentially more significant to trial 1 than to trial 2 since the lower concentration of alkyl radicals corresponds to a longer lifetime of the RO_2 radical for bimolecular reactions. Unimolecular isomerization will result in the formation of SA and lead to the seemingly higher branching ratios for Path 3(a) in trial 1 for both scenarios. The branching ratio calculated for the more reliable trial 2 is thus used in the following discussion. For these reasons, the MA mechanism (particularly the branching ratio values) is not as certain as the mechanisms determined for MVK and MBO.

A General Sulfate Radical Addition Mechanism. Based on the results from each system, summarized in Table S18, the fragmentation pathways, Paths 3(a) and 3(b), are the major pathways. The relative importance of Path 3(a) vs Path 3(b) is system-specific. In general, fragmentation pathways are preferred over the hydrogen abstraction by O_2 for alkoxy radicals directly derived from a precursor. Fragmentation to form a more substituted radical is preferred over the formation of a less substituted radical, which is consistent with the general trends observed in the gas phase.[30] Both Paths 1 and 2 were active in several systems, although Path 2 seems to be the more facile route of the two. Previous studies of gas-phase RO_2 + RO_2 branching ratios have found that electronegative functional groups seem to favor RO + RO pathways[23] (Paths 2 and 3 in our mechanism); thus, the neighboring electronegative sulfate groups may explain this preference. The uncertainty in the branching ratios calculated for the photochemical reactions was assumed to be around 10%, to account for the inaccuracies stemming from the integration of the overlapping signals and products that were not detected due to low concentrations.

A general sulfate radical addition mechanism is proposed in which the relative importance of each path is indicated by the size of the reaction arrow (Figure 5), as discussed above. In the generalized mechanism, the carbon atom with the R_3 and R_4 substituents is the less substituted side. Path 1, Path 2, and further oxidation steps are viable if R_1 and/or R_2 is a hydrogen atom, which is true for MVK and MBO. Here, R_2 is assumed to be a hydrogen atom. If neither R_1 nor R_2 is a hydrogen atom, which is the case in the MA system, another fragmentation pathway that is Path 3(a)-like is possible. Path 3(c) in the MA mechanism is an example of this fragmentation pathway.

Comparison to Previous Results. The produced organosulfate products from the sulfate radical reactions with MVK and MA were compared with previous results,[8,20,22,39,40] all of which used LC−MS as the characterization method. Among the five previous studies, only the work by Hettiyadura et al.[8] is a field investigation, and the rest are laboratory studies that used a single organic precursor in each experiment. The comparison of products detected from the sulfate radical

addition to MVK is listed in Table S19, and the comparison for sulfate addition to MA is listed in Table S20. Note that there are often multiple proposed structures for the same m/z or molecular formula, which is indicative of the general limitation of LC−MS in providing unambiguous structural information in the absence of standards.

For sulfate radical addition to MVK, m/z ratios corresponding to three out of the four organosulfate products of the MVK reaction were observed in LC−MS studies; Table S19 presents a full comparison. We detected GL-S in its hydrated form and attributed GL-S-OH to be a secondary product of GL-S oxidation in our mechanism. Most laboratory studies only observed GL-S-OH. The higher abundance of GL-S-OH in ambient aerosol suggests that this oxidation occurs rapidly in the atmosphere.[8] We did not detect DHBO-4-S (3-hydroxy-4-sulfate-2-butanone), which has been identified in several LC−MS studies. Given the reduced sensitivity of NMR compared to LC−MS, this may be because of the low concentration of DHBO-4-S, which suggests that the contribution of MVK to the formation of DHBO-4-S in the atmosphere may not be significant. Three different structural isomers have been proposed for the compound with $m/z = 199$, but we only identify one hydrated compound (which is not likely to be detected with the LC−MS methods, which measure analytes as gases only) with this corresponding m/z. Our mechanism does not offer any obvious formation pathway for sulfatoacetone ($m/z = 153$) and 4-sulfate-2-butanone ($m/z = 167$), although m/z ratios corresponding to these species have been reported in previous studies.[22,39]

The discrepancy between the species predicted by our mechanism for MA and previous studies is more significant than for the MVK system (Table S20). The only shared product observed is sulfatoacetone. According to our mechanism of sulfate radical addition to MA, none of the products will retain the carbon backbone of MA. It is possible that the compounds with 4 or more carbons in previous studies actually derive from low-oxygen oligomerization pathways. Because of the varying degree of agreement between the present NMR-based study and previous LC−MS-based work, further development of the sulfate radical anion mechanism would likely benefit from a combined approach.

Atmospheric Implications. The observation of several organosulfates formed from sulfate radical addition to the atmospherically abundant MVK and MA precursors in the present study that also match the corresponding m/z carriers observed in field studies[8] indicates that sulfate radical addition to olefinic VOCs could explain the formation of some organosulfates in SOA. The observation of the secondary oxidation of organosulfate products could explain the presence of small organosulfates, such as glycolic acid-2-sulfate (GL-S-OH) and lactic acid sulfate, in ambient SOA. Since no oligomers were identified in any of the present oxygen-saturated experiments, the observation of oligomers in some of the previous studies,[20,22] in which oxygen levels were not actively controlled, raises the question of whether sulfate-radical-initiated oligomerization is an atmospherically relevant process. The observation of small organic acids across all systems indicated that solution-phase radical-initiated oxidation of the BVOCs can also provide several formation pathways to the ubiquitous formic acids and acetic acids[41] in the atmosphere in addition to the known gas-phase oxidation routes. However, the contribution of this mechanism to organosulfate SOA formation is dependent on establishing the

importance of the sulfate radical as an important oxidant in the atmosphere, which remains uncertain.

■ ASSOCIATED CONTENT

ⓢ Supporting Information

The Supporting Information is available free of charge at https://pubs.acs.org/doi/10.1021/acs.est.0c05256.

UV−Vis data, NMR assignments, kinetics and product quantitation data, comparison to previous results (PDF)

■ AUTHOR INFORMATION

Corresponding Author

Matthew J. Elrod − *Department of Chemistry and Biochemistry, Oberlin College, Oberlin, Ohio 44074, United States;* ⊙ orcid.org/0000-0002-1656-8261; Email: mjelrod@oberlin.edu

Authors

He Ren − *Department of Chemistry and Biochemistry, Oberlin College, Oberlin, Ohio 44074, United States*

Jane A. Sedlak − *Department of Chemistry and Biochemistry, Oberlin College, Oberlin, Ohio 44074, United States*

Complete contact information is available at:
https://pubs.acs.org/10.1021/acs.est.0c05256

Notes

The authors declare no competing financial interest.

■ ACKNOWLEDGMENTS

■ REFERENCES

(1) Kroll, J. H.; Seinfeld, J. H. Chemistry of secondary organic aerosol: Formation and evolution of low-volatility organics in the atmosphere. *Atmos. Environ.* **2008**, *42*, 3593−3624.

(2) Kanakidou, M.; Seinfeld, J. H.; Pandis, S. N.; Barnes, I.; Dentener, F. J.; Facchini, M. C.; Van Dingenen, R.; Ervens, B.; Nenes, A.; Nielsen, C. J.; Swietlicki, E.; Putaud, J. P.; Balkanski, Y.; Fuzzi, S.; Horth, J.; Moortgat, G. K.; Winterhalter, R.; Myhre, C. E. L.; Tsigaridis, K.; Vignati, E.; Stephanou, E. G.; Wilson, J. Organic aerosol and global climate modelling: a review. *Atmos. Chem. Phys.* **2005**, *5*, 1053−1123.

(3) West, J. J.; Cohen, A.; Dentener, F.; Brunekreef, B.; Zhu, T.; Armstrong, B.; Bell, M. L.; Brauer, M.; Carmichael, G.; Costa, D. L.; Dockery, D. W.; Kleeman, M.; Krzyzanowski, M.; Künzli, N.; Liousse, C.; Lung, S. S.-C.; Martin, R. V.; Pöschl, U.; Pope, C. A., III; Roberts, J. M.; Russell, A. G.; Wiedinmyer, C. What We Breathe Impacts Our Health: Improving Understanding of the Link between Air Pollution and Health. *Environ. Sci. Technol.* **2016**, *50*, 4895−4904.

(4) Pope, C. A., III; Dockery, D. W. Health effects of fine particulate air pollution: lines that connect. *J. Air Waste Manage. Assoc.* **2006**, *56*, 709−742.

(5) Dockery, D. W.; Pope, C. A.; Xu, X.; Spenger, J. D.; Ware, J. H.; Fay, M. E.; Ferris, B. G., Jr.; Speizer, F. E. An association between air pollution and mortality in six U.S. cities. *N. Engl. J. Med.* **1993**, *329*, 1753−1759.

(6) Tolocka, M. P.; Turpin, B. Contribution of organosulfur compounds to organic aerosol mass. *Environ. Sci. Technol.* **2012**, *46*, 7978−7983.

(7) Hughes, D. D.; Christiansen, M. B.; Milani, A.; Vermeuel, M. P.; Novak, G. A.; Alwe, H. D.; Dickens, A. F.; Pierce, R. B.; Millet, D. B.; Bertram, T. H.; Stanier, C. O.; Stone, E. A. PM2.5 chemistry,

organosulfates, and secondary organic aerosol during the 2017 Lake Michigan Ozone Study. *Atmos. Environ.* **2021**, *244*, 117939.

(8) Hettiyadura, A. P. S.; Al-Naiema, I. M.; Hughes, D. D.; Fang, T.; Stone, E. A. Organosulfates in Atlanta, Georgia: anthropogenic influences on biogenic secondary organic aerosol formation. *Atmos. Chem. Phys.* **2019**, *19*, 3191−3206.

(9) Hettiyadura, A. P. S.; Xu, L.; Jayarathne, T.; Skog, K.; Guo, H.; Weber, R. J.; Nenes, A.; Keutsch, F. N.; Ng, N. L.; Stone, E. A. Source apportionment of organic carbon in Centreville, AL using organo-sulfates in organic tracer-based positive matrix factorization. *Atmos. Environ.* **2018**, *186*, 74−88.

(10) Hettiyadura, A. P. S.; Jayarathne, T.; Baumann, K.; Goldstein, A. H.; de Gouw, J. A.; Koss, A.; Keutsch, F. N.; Skog, K.; Stone, E. A. Qualitative and quantitative analysis of atmospheric organosulfates in Centreville, Alabama. *Atmos. Chem. Phys.* **2017**, *17*, 1343−1359.

(11) Surratt, J. D.; Gómez-González, Y.; Chan, A. W. H.; Vermeylen, R.; Shahgholi, M.; Kleindienst, T. E.; Edney, E. O.; Offenberg, J. H.; Lewandowski, M.; Jaoui, M.; Maenhaut, W.; Claeys, M.; Flagan, R. C.; Seinfield, J. H. Organosulfate formation in biogenic secondary organic aerosol. *J. Phys. Chem. A* **2008**, *112*, 8345−8378.

(12) Chan, M. N.; Surratt, J. D.; Chan, A. W. H.; Schilling, K.; Offenberg, J. H.; Lewandowski, M.; Edney, E. O.; Kleindienst, T. E.; Jaoui, M.; Edgerton, E. S.; Tanner, R. L.; Shaw, S. L.; Zheng, M.; Knipping, E. M.; Seinfeld, J. H. Influence of aerosol acidity on the chemical composition of secondary organic aerosol from β-caryophyllene. *Atmos. Chem. Phys.* **2011**, *11*, 1735−1751.

(13) Zhang, H.; Worton, D. R.; Lewandowski, M.; Ortega, J.; Rubitschun, C. L.; Park, J.-H.; Kristensen, K.; Campuzano-Jost, P.; Day, D. A.; Jimenez, J. L.; Jaoui, M.; Offenberg, J. H.; Kleindienst, T. E.; Gilman, J.; Kuster, W. C.; de Gouw, J.; Park, C.; Schade, G. W.; Frossard, A. A.; Russell, L.; Kaser, L.; Jud, W.; Hansel, A.; Cappellin, L.; Karl, T.; Glasius, M.; Guenther, A.; Goldstein, A. H.; Seinfeld, J. H.; Gold, A.; Kamens, R. M.; Surratt, J. D. Organosulfates as tracers for secondary organic aerosol (SOA) formation from 2-methyl-3-buten-2-ol (MBO) in the atmosphere. *Environ. Sci. Technol.* **2012**, *46*, 9437−9446.

(14) Paulot, F.; Crounse, J. D.; Kjaergaard, H. G.; Kurten, A.; St. Clair, J. M.; Seinfeld, J. H.; Wennberg, P. O. Unexpected epoxide formation in the gas-phase photooxidation of isoprene. *Science* **2009**, *325*, 730−733.

(15) Darer, A. I.; Cole-Filipiak, N. C.; O'Connor, A. E.; Elrod, M. J. Formation and stability of atmospherically relevant isoprene-derived organosulfates and organonitrates. *Environ. Sci. Technol.* **2011**, *45*, 1895−1902.

(16) Surratt, J. D.; Chan, A. W. H.; Eddingsaas, N. C.; Chan, M.; Loza, C. L.; Kwan, A. J.; Hersey, S. P.; Flagan, R. C.; Wennberg, P. O.; Seinfeld, J. H. Reactive intermediates revealed in secondary organic aerosol formation from isoprene. *Proc. Natl. Acad. Sci.* **2010**, *107*, 6640−6645.

(17) Kwong, K. C.; Chim, M. M.; Davies, J. F.; Wilson, K. R.; Chan, M. N. Importance of sulfate radical anion formation and chemistry in heterogeneous OH oxidation of sodium methyl sulfate, the smallest organosulfate. *Atmos. Chem. Phys.* **2018**, *18*, 2809−2820.

(18) Chen, Y.; Zhang, Y.; Lambe, A. T.; Xu, R.; Lei, Z.; Olson, N. E.; Zhang, Z.; Szalkowski, T.; Cui, T.; Vizuete, W.; Gold, A.; Turpin, B. J.; Ault, A. P.; Chan, M. N.; Surratt, J. D. Heterogeneous Hydroxyl Radical Oxidation of Isoprene-Epoxydiol-Derived Methyltetrol Sulfates: Plausible Formation Mechanisms of Previously Unexplained Organosulfates in Ambient Fine Aerosols. *Environ. Sci. Technol. Lett.* **2020**, *7*, 460−468.

(19) Rudziński, K. J.; Gmachowski, L.; Kuznietsova, I. Reactions of isoprene and sulphoxy radical-anions - a possible source of atmospheric organosulphites and organosulphates. *Atmos. Chem. Phys.* **2009**, *9*, 2129−2140.

(20) Nozière, B.; Ekström, S.; Alsberg, T.; Holmström, S. Radical-initiated formation of organosulfates and surfactants in atmospheric aerosols. *Geophys. Res. Lett.* **2010**, *37*, L05806.

(21) Schöne, L.; Schindelka, J.; Szeremeta, E.; Schaefer, T.; Hoffmann, D.; Rudzinski, K. J.; Szmigielski, R.; Herrmann, H.

Atmospheric aqueous phase radical chemistry of the isoprene oxidation products methacrolein, methyl vinyl ketone, methacrylic acid and acrylic acid–kinetics and product studies. *Phys. Chem. Chem. Phys.* **2014**, *16*, 6257−6272.

(22) Schindelka, J.; Iinuma, Y.; Hoffmann, D.; Herrmann, H. Sulfate radical-initiated formation of isoprene-derived organosulfates in atmospheric aerosols. *Faraday Discuss.* **2013**, *165*, 237.

(23) Orlando, J. J.; Tyndall, G. S. Laboratory studies of organic peroxy radical chemistry: an overview with emphasis on recent issues of atmospheric significance. *Chem. Soc. Rev.* **2012**, *41*, 6294.

(24) Hettiyadura, A. P. S.; Stone, E. A.; Kundu, S.; Baker, Z.; Geddes, E.; Richards, K.; Humphry, T. Determination of atmospheric organosulfates using HILIC chromatography with MS detection. *Atmos. Meas. Tech.* **2015**, *8*, 2347−2358.

(25) Cui, T.; Zeng, Z.; dos Santos, E. O.; Zhang, Z.; Chen, Y.; Zhang, Y.; Rose, C. A.; Budisulistiorini, S. H.; Collins, L. B.; Bodnar, W. M.; de Souza, R. A. F.; Martin, S. T.; Machado, C. M. D.; Turpin, B. J.; Gold, A.; Ault, A. P.; Surratt, J. D. Development of a hydrophilic interaction liquid chromatography (HILIC) method for the chemical characterization of water-soluble isoprene epoxydiol (IEPOX)-derived secondary organic aerosol. *Environ. Sci.: Processes Impacts* **2018**, *20*, 1524−1536.

(26) Van Buren, J.; Prasse, C.; Marron, E. L.; Skeel, B.; Sedlak, D. L. Ring-Cleavage Products Produced during the Initial Phase of Oxidative Treatment of Alkyl-Substituted Aromatic Compounds. *Environ. Sci. Technol.* **2020**, *54*, 8352−8361.

(27) Penn, J. H.; Orr, R. D. A microscale immersion well for photochemical reactions. *J. Chem. Educ.* **1989**, *66*, 86.

(28) Yamaji, T.; Saito, T.; Hayamizu, K.; Yanagisawa, M.; Yamamoto, O. *Spectral Database for Organic Compounds, SDBS*; National Institute of Advanced Industrial Science and Technology (AIST): Japan.

(29) Minerath, E. C.; Schultz, M. P.; Elrod, M. J. Kinetics of the reactions of isoprene-derived epoxides in model tropospheric aerosol solutions. *Environ. Sci. Technol.* **2009**, *43*, 8133−8139.

(30) Seinfeld, J. H.; Pandis, S. N. *Atmospheric chemistry and physics*; 3rd ed.; John Wiley and Sons, Inc.: New Jersey, 2016.

(31) Galloway, M. M.; Huisman, A. J.; Yee, L. D.; Chan, A. W. H.; Loza, C. L.; Seinfeld, J. H.; Keutsch, F. N. Yields of oxidized volatile organic compounds during the OH radical initiated oxidation of isoprene, methyl vinyl ketone, and methacrolein under high-NOx conditions. *Atmos. Chem. Phys.* **2011**, *11*, 10779−10790.

(32) House, D. A. Kinetics and Mechanism of Oxidations by Peroxydisulfate. *Chem. Rev.* **1962**, *62*, 185−203.

(33) Carrasco, N.; Doussin, J. F.; O'Connor, M.; Wenger, J. C.; Picquet-Varrault, B.; Durand-Jolibois, R.; Carlier, P. Simulation Chamber Studies of the Atmospheric Oxidation of 2-Methyl-3-Buten-2-ol: Reaction with Hydroxyl Radicals and Ozone Under a Variety of Conditions. *J. Atmos. Chem.* **2007**, *56*, 33−55.

(34) Mael, L. E.; Jacobs, M. I.; Elrod, M. J. Organosulfate and nitrate formation and reactivity from epoxides derived from 2-methyl-3-buten-2-ol. *J. Phys. Chem. A* **2015**, *119*, 4464−4472.

(35) Calvert, J.; Mellouki, A.; Orlando, J. *The mechanisms of atmospheric oxidation of the oxygenates*; Oxford University Press: New York, 2011.

(36) Crounse, J. D.; Nielsen, L. B.; Jørgensen, S.; Kjaergaard, H. G.; Wennberg, P. O. Autoxidation of Organic Compounds in the Atmosphere. *J. Phys. Chem. Lett.* **2013**, 3513−3520.

(37) Orlando, J. J.; Tyndall, G. S.; Paulson, S. E. Mechanism of the OH-initiated oxidation of methacrolein. *Geophys. Res. Lett.* **1999**, *26*, 2191−2194.

(38) Schmidt, M.; Jansen van Beek, S. M.; Abou-Ghanem, M.; Oliynyk, A. O.; Locock, A. J.; Styler, S. A. Production of Atmospheric Organosulfates via Mineral-Mediated Photochemistry. *ACS Earth Space Chem.* **2019**, *3*, 424−431.

(39) Wach, P.; Spólnik, G.; Rudziński, K. J.; Skotak, K.; Claeys, M.; Danikiewicz, W.; Szmigielski, R. Radical oxidation of methyl vinyl ketone and methacrolein in aqueous droplets: Characterization of

organosulfates and atmospheric implications. *Chemosphere* **2019**, *214*, 1−9.

(40) Huang, L.; Coddens, E. M.; Grassian, V. H. Formation of Organosulfur Compounds from Aqueous Phase Reactions of S(IV) with Methacrolein and Methyl Vinyl Ketone in the Presence of Transition Metal Ions. *ACS Earth Space Chem.* **2019**, *3*, 1749−1755.

(41) Link, M. F.; Nguyen, T. B.; Bates, K.; Müller, J.-F.; Farmer, D. K. Can Isoprene Oxidation Explain High Concentrations of Atmospheric Formic and Acetic Acid over Forests? *ACS Earth Space Chem.* **2020**, *4*, 730−740.